

# **Crystallite size and Solid Solubility Cr to Fe analysis of Fe<sub>80</sub>Cr<sub>20</sub> Interconnect Material Treated by Ultrasonic and High Energy Ball milling Process**

**By**

**Imam Hidayat, Dafit Feriyanto**

Department of Mechanical Engineering, Faculty of Engineering, Universitas Mercu Buana, Jakarta, Indonesia

**Hadi Pranoto and Gian Villani Golwa**

Department of Mechanical Engineering, Faculty of Engineering, Universitas Mercu Buana, Jakarta, Indonesia

**Supaat Zakaria**

Department of Mechanical Engineering, Politeknik Ungku Omar, Jalan Raya Musa Mahadi 1400, Ipoh, Perak, Malaysia.

Email: [imam.hidayat@mercubuana.ac.id](mailto:imam.hidayat@mercubuana.ac.id)

## **Abstract**

In the current research, there is high interest in nanocrystalline iron and chromium based alloys. The iron-chromium has long been used by many engineering alloys as basis in high-strength and corrosion-resistant applications such as for fuel cell interconnect. The problem is there is high crystalline growth at high temperature operation up to 1000 °C. Therefore, this research investigates the crystallite size and solid solubility of the Fe<sub>80</sub>Cr<sub>20</sub> metallic material that projected have high thermal stability to applied as Interconnect fuel cell. The method of this research was conducted through high energy milling for 60 h and ultrasonic bath by frequency of 35 kHz and various holding time of 3, 3.5, 4, 4.5 and 5 h. The analysis of the crystallite size and solid solubility were conducted by X-Ray Diffraction (XRD) with diffraction angle of 10-90° and operation time of 25 minutes. High energy ball milling is the most effective technique to reduce the crystallite size up to 96 % and it combined with ultrasonic achieve 2.171 nm crystallite size and improve the solid solubility up to 86.4 % as compared to the raw material. These results achieved high energy kinetics and the ball slugging the powder during ball milling process.

## **Background Motivation and Objective**

The interconnect is required to connect thermally the different cells and also provides the physical barriers to keep the oxidant and fuel separated (Yaodong *et al.*, 2007). Metallic materials are easier for machining, easier and cheaper to fabricate as well as they are less brittle than ceramic material (Khaerudini *et al.*, 2012). If compared with ceramic interconnect, the metallic interconnect can reduce the fabrication cost, facilitate the production of more complex fuel cell designs and improve the efficiency of the fuel cell (Benjamin, 2004). Developing alloys metal with chromium, aluminium and silicon encourage the formation of protective oxide (scales) of chromia, alumina and silica, respectively. Iron (Fe) as metallic interconnect has many advantages such as good work ability, low cost and thermal expansion coefficient similar with other cell component. Chromium is formed on the surface during vaporization operation and it decreases the cathode activity. However, the chromium based alloys have some weaknesses such as formation of volatile Cr(VI) which occur under operating

environment of SOFC (Jong-Hee Kim *et al.*, 2004). Fe-16Cr alloys (SUS430) have been studied on oxidation kinetics under the condition of the air and fuel side environments in SOFC application (Hideto *et al.*, 2004). The growth rate scale in the air and fuel side is almost same when it reaches the temperature of 1073 K (Hideto *et al.*, 2004). In the air side, the growth rate of iron oxide is higher than in the steam side. It might be caused by the hydrogen permeates from the effect of oxidation behaviour on the steam side. Interconnect of SOFC is exposed simultaneously both of air and full atmospheres. The summaries of the description of the metallic materials for interconnect are listed in Table 1.

**Table 1** *Varies metallic candidate materials for interconnect application*

No.	Author	Metallic material for interconnect	Analyzed to
1	Hendi, 2011 Ade, 2012	Fe <sub>80</sub> Cr <sub>20</sub> FeCrAl	<ul style="list-style-type: none"> <li>Investigate the crystallite size, oxidation kinetics, CTE, electrical properties, morphology and composition analysis.</li> <li>The distribution of particle size, morphology, and oxidation kinetics.</li> </ul>
2	Quadackers <i>et al.</i> , 2003	MnCrAl	Investigate the excellent oxidation protection of the alumina scale
3	Jong-Hee Kim <i>et al.</i> , 2004	iron, nickel, cobalt, chromium, aluminium and silicon	Investigate the electrical conductivity.
4	<ul style="list-style-type: none"> <li>Hideto <i>et al.</i>, 2004</li> <li>Murugesan <i>et al.</i>, 1999</li> <li>Rajeev <i>et al.</i>, 2013</li> </ul>	Fe-16Cr alloys (SUS430) Fe <sub>1-x</sub> Cr <sub>x</sub> Fe <sub>20</sub> Cr Alloy	<ul style="list-style-type: none"> <li>Investigate the oxidation kinetics</li> <li>Investigate the magnetism of nanocrystalline alloys</li> <li>Investigate the corrosion rate or corrosion resistance</li> </ul>
5	Geng <i>et al.</i> , 2006	Ni-based alloy Haynes 242 and Ebrite and Haynes 230	Investigate the parabolic law and weight gain.
6	Zhenguang Yang <i>et al.</i> , 2006	Haynes 230, Hastelloy S and Haynes 242	Investigate the oxidation behaviour, scale conductivity and thermal expansion

The Fe-Cr phase diagram is shown in Figure 1 (ASM Handbook, 1992). At low temperatures, chromium and iron do not form a complete solid solution due to the presence of the sigma phase ( $\sigma$ -phase) which has a tetragonal structure and generally it is hard and brittle. The equilibrium phase diagram predicts the formation of  $\sigma$ -phase for alloys containing greater than 15 wt% Cr at temperatures among 475<sup>o</sup>C and 821<sup>o</sup>C. However, heat-treatments at high temperatures and long holding time or slow cooling rates are required for the formation of this phase (Dafit Feriyanto and Supaat Zakaria, 2020). For a Fe 27 wt% Cr alloy, it was shown that  $\sigma$ -phase would precipitate out of the  $\sigma$ -phase after holding at 565<sup>o</sup>C for 131 days. A Fe-20 wt% Cr alloy, held in temperatures of 600<sup>o</sup>C and above as shown in Figure 1, it would be within the  $\alpha$ -phase field and would never form  $\sigma$ -phase after extended the high temperature exposure (Benjamin, 2004).

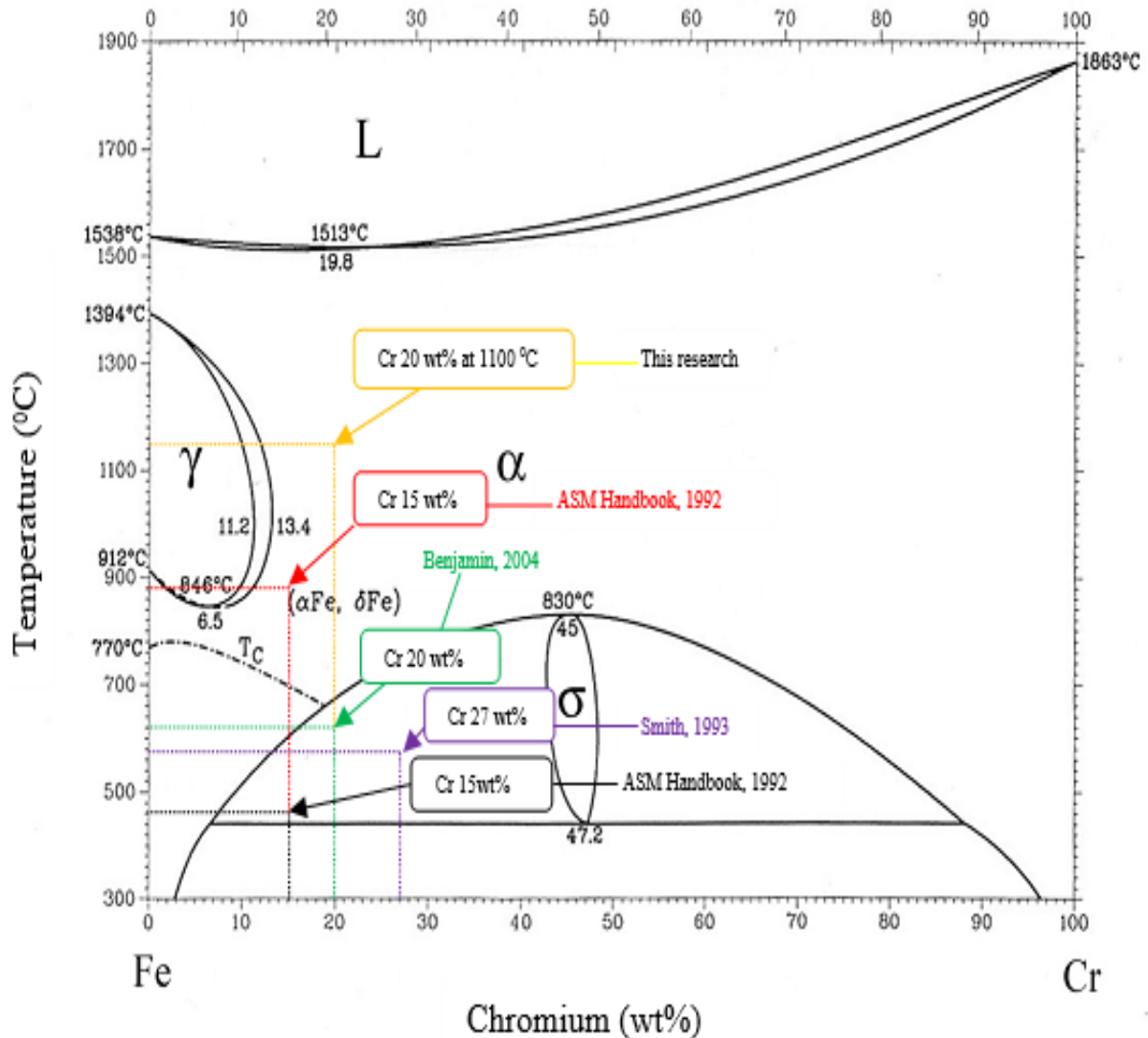


**Figure 1.** Phase diagram of Fe-Cr system (ASM Handbook, 1992)

From Figure 1, it can be seen that this research study in composition of 80 wt% Fe and 20 wt% Cr in 1100°C temperature operation for thermal analysis. That area was designed because the high ductile and strength  $\alpha$ -phase will be obtained that influenced by crystallite size and its physical properties (Dafit Feriyanto *et al.*, 2020). Therefore, this research has main objective to investigate the crystallite size and solid solubility Cr to Fe analysis that influence to the physical properties of the fuel cell interconnector.

## Methods

The treatments that performed to the  $Fe_{80}Cr_{20}$  is high energy ball milling to reduce the crystallite size and ultrasonic technique to breaking the agglomerates. The material for high energy ball milling was prepared by glovebox machine with the pressure of 2000 psi with 20 psi of nitrogen pressure. The  $Fe_{80}Cr_{20}$  material was milled by planetary ball mill for 60 h and the setting was  $300 \text{ rpm} \pm 2 \text{ rpm}$ , 10 minutes pause time and 30 minutes cycle time. Meanwhile, the preparation process of ultrasonic is the sample put into the jar and it placed into ultrasonic machine. The water was used as liquid media for spreading the ultrasonic waves. The ultrasonic use the frequency of 35kHz and various ultrasonic time of 3, 3.5, 4, 4.5 and 5 h. The schematic diagram of ultrasonic process is shown in Figure 2.

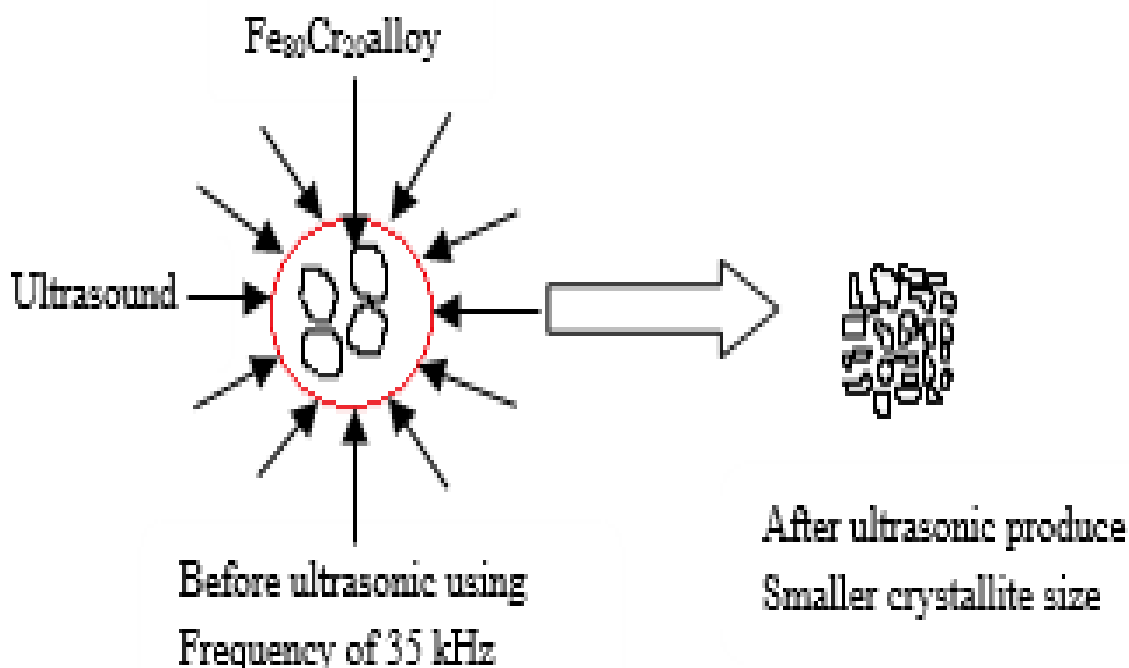


**Figure 2.** Schematic diagram of ultrasonic process to breaking the agglomerates

XRD was employed to analyze the surface of the Fe<sub>80</sub>Cr<sub>20</sub> by using Copper (Cu) (1.54 Å). XRD data is obtained by using X'pert data collector software. Data analysis obtained by using X'pert Highscore and X'pert data viewer. XRD was conducted by diffraction angle of 10 – 90 degree for the operation time of 25 minutes. The crystallite size (D) of treated and untreated Fe<sub>80</sub>Cr<sub>20</sub> alloy powder is estimated from the Scherrer's method as shown in equation 1:

$$D = \frac{k * \lambda}{B \cos \theta} \quad (1)$$

Where, D = The crystallite size (nm)

k = The shape factor (K=0.9)

$\lambda$  = Wavelength of the X-Ray ( $\lambda=0.154056$  nm for Cu-K  $\alpha$ )

$\theta$  = Bragg diffraction angle

B = The broadening of the diffraction peak measured at half of its maximum intensity (rad) (Mittemeijer *et al.*, 2008).

Williamson-Hall size-strain analysis was developed in 1953 as a method to separate size and strain effect by their angular dependence (Mittemeijer *et al.*, 2008 and Ungar *et al.*, 2001).

$$\partial(2\theta) \cos \theta = \frac{k * \lambda}{D} + 4\epsilon \sin \theta \quad (2)$$

Where; D = The crystallite size (nm)

$\partial(2\theta)$  = FWHM (rad)

## Results and Discussions

### *Determining crystallite size using Williamson-Hall method*

Crystallite size of the material can be calculated by using these two (2) equations which are Scherrer formula (equation 1) and Williamson-Hall formula (equation 2). Scherrer equation method is used for the estimation of particle size does not take from the broadening account since the lattice present in the samples. However, in the present investigation, the lattice strains have been estimated using Williamson-Hall method. It assumed that the crystallite size and strain are similar nature. The intersection with the vertical axis ( $\frac{k\lambda}{FWHM} + 4\varepsilon \sin \theta$ ) is estimated become the crystallite size (D) and the strain ( $\varepsilon$ ) using equation 2.14 (Page 46) which is estimated from the slop of the line (Huub, 2005 and Williamson 1953). Prior to obtaining the crystallite size, the most important thing is determining the variable which is used to calculate the crystallite size. Based on XRD data for treated and untreated samples, it is possible to calculate the  $B_{corrected}$  (The instrumental corrected full width at half maximum (FWHM) is located at  $2\theta$  (rad)), lattice parameter ( $a$ ) and interplanar spacing ( $d$ ). The complete calculation can be seen in appendix A and presented as in Table 2.

**Table 2** Result of XRD analysis of the treated and untreated samples

Sample designation	$B_{corrected}$ (rad)	Lattice parameter "a" (Å)	Increasing lattice parameter	Interplanar spacing "d" (Å)	Increasing interplanar spacing
Fe <sub>80</sub> Cr <sub>20</sub>	0.0147	2.863		1.542	
UT 3 h	0.0152	2.863	0.002 Å	1.542	0.001 Å
UT 3.5 h	0.0142	2.864	when	1.542	when
UT 4 h	0.0134	2.864	compare	1.543	compare
UT 4.5 h	0.0173	2.865	d to raw	1.543	d to raw
UT 5 h	0.0181	2.865	material	1.543	material
milled 60 h	0.0172	2.868	0.005 Å when compare d to UT sample	1.546	0.004 Å when compare d to UT sample
milled and UT 3 h	0.0141	2.868	0.007 Å, 0.007 Å	1.545	0.005 Å, 0.005 Å
milled and UT 3.5 h	0.0236	2.869	and 0.002 Å	1.544	and 0.001 Å
milled and UT 4 h	0.0171	2.87	when compare	1.545	when compare
milled and UT 4.5 h	0.0181	2.87	d to raw material, UT	1.546	d to raw material, UT
milled and UT 5 h	0.0161	2.87	samples, milled 60 h sample, respectiv ely	1.547	samples, milled 60 h sample, respectiv ely

Raw material with smaller lattice parameter have a sharpest peaks since the grain size still in micrometer and have irregular round shape which caused good inter-particle bonding. The irregular shapes produce the good interparticle bonding. The irregular round shape and rough surface is observed in raw material and after ball milling process lead to good consolidated materials but some void has observed (Hendi, 2011 and Deni, 2011). Therefore, finer surface morphology is suggested to obtain better consolidated material (Yanuandri, 2011; Ade, 2012 and Rajeev *et al.*, 2013).

Comparison of sample designation on lattice parameter ( $a$ ) and inter-planar spacing ( $d$ ) is shown in Table 2. Influence of the low frequency ultrasonic process, ball milling process and combination technique was provided to increase the lattice parameter ( $a$ ) and inter-planar spacing ( $d$ ). Lattice parameter ( $a$ ) is in line with the inter-planar spacing ( $d$ ). Therefore, if the lattice parameter increases, the inter-planar spacing will increase as well. From the B (FWHM of reflection peaks located at  $2\theta$  (rad)), lattice parameter ( $a$ ) and inter-planar spacing ( $d$ ) value, possible to calculate the solid solubility ( $x_{ss}$ ), crystallite size ( $D$ ) and strain ( $\epsilon$ ) of the materials.

### ***Correlation between crystallite size and solid solubility***

In the UT samples, milled 60 h and combination treatment (milled and UT) samples with the ultrasonic time of 3 h, 3.5 h, 4 h and 4.5 h have influenced to the increases of the solid solubility. However, the solid solubility in ultrasonic time of 5 h shows conversely. Consequently, this solid solubility of the combination technique (milled and UT) samples are better than raw material, UT samples and milled 60 h sample. It was proved by solid solubility of the combination technique (milled and UT) which is increased up to 90.1 % as compared to raw material, 64.8 % as compared to ultrasonic (UT) samples and 29.5 % as compared to milled 60 h sample. It shown the combination technique was effective to produce the solubility of Cr powder to Fe powder. Formation of solid solubility is dependent on the temperature ball milling. When the  $Fe_{80}Cr_{20}$  dissolves in a ball milling machine and ultrasonic machine temperature has increased, the average kinetic energy of the  $Fe_{80}Cr_{20}$  alloy powder also increases. The increasing of kinetic energy allows the solvent molecules are more effective to break apart the solute molecules that are held together by intermolecular attractions (Dafit Feriyanto *et al.*, 2021).

**Table 3.** *Crystallite size and solid solubility of the treated and untreated samples*

<b>Sample designation</b>	<b>Crystallite size (D) (nm)</b>	<b>The solubility Cr into Fe (%)</b>
$Fe_{80}Cr_{20}$	138.656	3.569
UT 3 h	69.33	3.773
UT 3.5 h	57.776	6.997
UT 4 h	42.019	7.266
UT 4.5 h	37.477	13.077
UT 5 h	37.991	10.478
milled 60 h	5.549	26.210
milled and UT 3 h	4.477	27.198
milled and UT 3.5 h	3.966	29.023
milled and UT 4 h	2.241	33.836
milled and UT 4.5 h	2.171	37.174
milled and UT 5 h	3.856	36.870

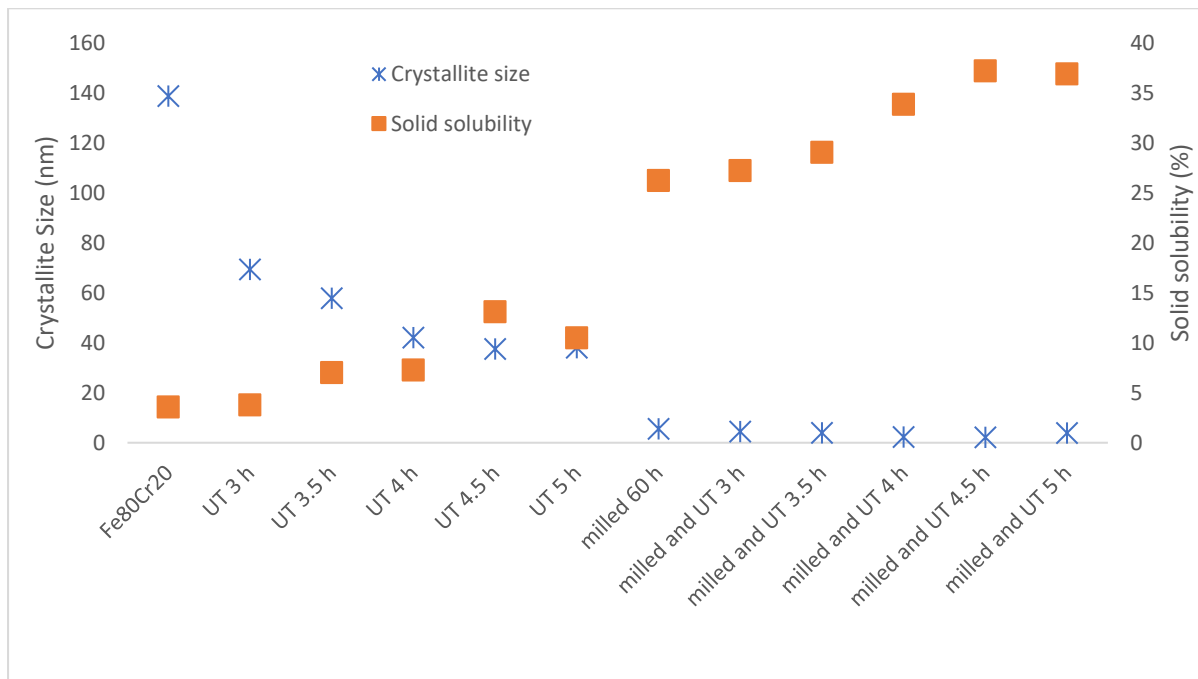


**Figure 3.** Crystallite size and solid solubility of treated and untreated samples

From the measurement of the crystallite size using Williamson-Hall method, it was observed the comparison of percentage of the decreasing crystallite size of treated and untreated sample and listed as in Table 4.

**Table 4.** Comparison crystallite size of the treated and untreated samples

No.	Sample name	Reduction of crystallite size (%)	Comparison
1.	UT samples	73	Raw material
2.	Milled 60 h	i.96 ii.92	i.Raw material ii.UT samples
3.	Combination technique samples	i.61 ii.96 iii.98	i.Milled 60 h sample ii.UT samples iii.Raw material

It was found that the combination technique (milled and UT) has a significant effect in reducing the crystallite size. Higher percentage value of the decreasing crystallite size of the combination technique samples is due to the Fe<sub>80</sub>Cr<sub>20</sub> alloy powder with the crystallite size is smaller than 20 nm, therefore total crystalline volume fractions of inter-crystalline region become significant (Schmidt *et al.*, 2013). Subsequently, the full dense material in the nanocrystalline material is developed. Crystallite size and strain on raw material until combination technique (milled and UT 4.5 h) samples are located in deformation elastic of material (continuous condition). It means the deformations which are recovered after the stress field has been removed. Meanwhile, the plastic deformation of the material is located at milled and UT 5 h (discontinuous condition). It means that the deformation of the material was discovered after stress fields or the plastic deformation occurred in material bodies after stresses have attained a certain threshold value and known as the elastic limit or yield stress. This behavior is caused by slip or dislocation mechanisms at the atomic level. It is supported by Lyubenova *et al.*, (2011) that the larger strain and smaller crystallite size started to grow as the temperature raise during ball milling and ultrasonic process.

## Conclusions

High energy ball milling to develop Fe<sub>80</sub>Cr<sub>20</sub> alloys with milling time of 60 h was successfully investigated as the most effective technique to reduce the crystallite size up to 96 % and to improve the solid solubility up to 86.4 % as compared to the raw material. These results are obtained since high energy kinetics and the ball slugging the powder during ball milling process. All the results produced by optimal combination between ball milling and ultrasonic treatment time to treat the Fe<sub>80</sub>Cr<sub>20</sub> alloy powder in obtaining the appropriate metallic material for interconnect in high temperature application

## Acknowledgments

The authors acknowledge Universitas Mercu Buana for funding support and lab facility. Special thanks to those who contributed to this project directly or indirectly.

## References

- Ade, F. (2012). *Ultrasonic treatment with nickel electroplating combined with oxidation for developing gamma alumina washcoat on Fe-Cr-Al substrate*. Universiti Tun Hussein Onn Malaysia, Malaysia: Master Thesis.
- ASM Handbook. (1992). *Alloy Phase Diagrams*. Materials Park, Vol. 3, OH: ASM International.
- Benjamin, C. C. (2004). *Fabrication and characterization of solid oxide fuel cell interconnect alloys*. Georgia Institute of Technology Atlanta, Georgia: Phd thesis.
- Dafit Feriyanto and Supaat Zakaria. (2020). New Method of Fabrication of Fe<sub>80</sub>Cr<sub>20</sub> Alloy: Effect of its Technique on Crystallite Size and Thermal Stability. *International Journal of Advanced Technology in Mechanical, Mechatronics and Materials*. Vol 1, No.1, pp. 26-31.
- Dafit Feriyanto, H Pranoto, H Carles and AM Leman. (2020). Comparison of metallic (FeCrAl) and Ceramic Catalytic Converter (CATCO) in reducing exhaust gas emission of gasoline engine fuelled by RON 95 to develop health environment. *IOP Conference Series: Earth and Environmental Science*. Vol. 485, No.1, p. 012004.
- Dafit Feriyanto and Samir Sani Abdul Malik, Muhamad Fitri, Imam Hidayat, Hadi Pranoto, Supaat Zakaria. (2021). Effect of Material Composition on Thermal Stability Analysis of Coated and Uncoated FeCrAl CATCO by  $\gamma$ -Al<sub>2</sub>O<sub>3</sub> Ultrasonic-Electroplating Technique. *Journal of Sustainable Materials Processing and Management*. Vol 1, No.1, pp. 1-7.
- Geng S. J., Zhu, J. H., and Lu, Z. G. (2006). Evaluation of Haynes 242 alloy as SOFC interconnect material. *Solid State Ionics*, 177, pp. 559 – 568.
- Hendi, S., Deni, S. K., Untoro, P., and Saleh, M. H. (2010). Determination of nanocrystalline Fe<sub>80</sub>Cr<sub>20</sub> based alloys using Williamson-hall Methode. *Advanced Materials Research*, 129-131, pp. 999-1003.
- Hideto, K., Kenichi, K., Toshio, M. (2004). Oxidation behavior of Fe–16Cr alloy interconnect for SOFC under hydrogen potential gradient. *Solid State Ionics*, 168, pp. 13–21.
- Jong-Hee, K., Rak-Hyun, S., and Sang-Hoon, H. (2004). Effect of slurry-coated LaSrMnO<sub>3</sub> on the electrical property of Fe–Cr alloy for metallic interconnect of SOFC. *Solid State Ionics*, 174, pp. 185–191.
- Khaerudini, D. S., Sebayang, D., Mahzan, S., and Untoro, P. (2012). Thermal stability of nanostructured iron–chromium alloys for interconnect application of solid oxide fuel cells *Corrosion Engineering, Science and Technology*, vol 47, no 7.

- Lyubenova, L., Spassov, T., and Spassova, M. (2011). Amorphization and solid solution formation in Sn modified Cu-Ag alloys produced by mall milling. *Bulgarian Chemical Communications*, Vol. 43, No. 2, pp. 288–292.
- Mittemeijer, E. J. and Welzel, U. (2008). The "State of The Art" of the diffraction analysis of crystallite size and lattice strain. *Z. Kristallogr*, Vol. 233, pp. 552-560.
- Murugesan, M., and Kuwano, H. (1999). Magnetic Properties of nano-crystalline Fe-Cr alloys prepared by mechanical alloying. *IEEE Transactions on Magnetics*, Vol 35, No 5.
- Quadackers, W. J., Piron, A. J., Shemet, V., and Singheiser, L. (2003). Metallic interconnector for solid oxide fuel cells-a review. Forschungszentrum Julich, IWV 2, 52425 Julich, MAHT/Quadackers, pp. 115-127.
- Rajeev, K. G., Singh, R. R. K., Carl, C. K., and Murti, B.S. (2013). Effect of Nanocrystalline Structure on the Corrosion of a Fe<sub>20</sub>Cr Alloy. *Int. J. Electrochem. Sci.*, 8, pp. 6791 – 6806.
- Schmidt K. J., Lin Y., Beaudoin M., Xia G., O'Leary S. K., Yue G., and Yan B. (2013). The dependence of the crystalline volume fraction on the crystallite size for hydrogenated nanocrystalline silicon based solar cells. *MRS proceedings*, Vol. 1536, pp. 113-118.
- Yanuandri, P. (2011). *Preparation of nio catalyst on FeCrAl substrate using various techniques at higher oxidation process*. Universiti Tun Hussein Onn Malaysia, Malaysia: Master Thesis.
- Yaodong, L., and Wei, L. (2007). Mechanical alloying and spark plasma sintering of the intermetallic compound Ti<sub>50</sub>Al<sub>50</sub>. *Journal of Alloys and Compounds*, Vol. 440, pp. 154–157.
- Zhenguo, Y., Guan-Guang, X., and Jeffry, W. S. (2006). Evaluation of Ni–Cr-base alloys for SOFC interconnect applications. *Journal of Power Sources*, 160, pp. 1104–1110.